Lasers in Manufacturing Conference 2017

Processing of a high-strength Al-Fe-Ni alloy using laser beam melting and its potential for in-situ graded mechanical properties

Gunther Mohr[a,*], Jan Johannsen[a], Daniel Knoop[b], Eric Gärtner[c], Klaus Hummert[d], Claus Emmelmann[a,e]

[a]*Hamburg University of Technology, Institute of Laser and System Technologies iLAS, Am Schleusengraben 14, 21029 Hamburg, Germany*
[b]*Stiftung Institut für Werkstofftechnik IWT, Badgasteiner Str. 3, 28359 Bremen, Germany,*
[c]*University of Bremen, Department of Production Engineering, Particle and Process Engineering, Badgasteiner Str. 1-3, 28359 Bremen, Germany*
[d]*Powder Light Metals GmbH, Am Wiesenbusch 2, 45966 Gladbeck, Germany*
[e]*LZN Laser Zentrum Nord GmbH, Am Schleusengraben 14, 21029 Hamburg, Germany*

Abstract

Laser beam melting (LBM) is a promising manufacturing technology for production of lightweight high quality parts. Due to the layer-wise fusion of metallic powder it offers outstanding opportunities for topology optimised designs and complex structures. One of the key challenges for further expansion of additive manufactured applications is to broaden the spectrum of suitable materials for the process. Especially within the class of aluminium alloys there is a lack of suitable high-strength alloys complementing prevalent aluminium-silicon casting alloys such as AlSi10Mg or AlSi12. The paper portrays the successful LBM processing of a high-strength Al-Fe-Ni alloy, which is usually used by extrusion in conventional manufacturing. In addition to the development of applicable process parameters for the production of high-density and crack free samples, mechanical properties are presented. Furthermore, the microstructure is discussed. Finally, the potential for manufacturing structures with graded mechanical properties is demonstrated by samples with particular gradients of hardness dependent on processing parameters.

Keywords: Additive Manufacturing (AM); Selective Laser Melting (SLM); Laser Beam Melting (LBM); high-strength aluminium alloys; metal powder

* Corresponding author. Tel.: +49 (0)40 484010-725; fax: +49 (0)40 484010-999.
E-mail address: gunther.mohr@tuhh.de.

1. Introduction

Additive Manufacturing (AM) technologies offer outstanding opportunities for production of complex and lightweight structures as well as functional and integral designs, Kranz et al., 2015, Karg et al., 2015, Spierings et al., 2016. Within AM technologies Laser Beam Melting (LBM) can be categorised as one of the most important ones, Herzog et al., 2016. Among other names Selective Laser Melting (SLM) is an often used synonym for LBM. There are several materials available for robust LBM processing comprising steels, titanium and aluminium, Herzog et al., 2016. However, qualifying new materials for reliable process conditions in order to broaden the spectrum of applications is still a key challenge. Especially within the class of aluminium alloys there is a lack of suitable high-strength alloys complementing prevalent aluminium-silicon casting alloys such as AlSi10Mg or AlSi12. To date only a Al-Mg-Sc alloy has caught relevant attention within the group of high strength Aluminium alloys, Schmidtke et al., 2011, Spierings et al., 2016. Further investigations on new Aluminium alloys have the potential to bridge this gap and to broaden the understanding of alloy composition requirements for specific LBM alloys.

2. Materials and methods

2.1. LBM-Process

LBM is a powder bed based process. Thin layers of a metal powder coated on a substrate plate are selectively exposed to laser radiation in order to melt and rapidly solidify the given alloy composition, generating material cohesion according to geometrical information of a sliced 3D-CAD-volume. The process sequence as well as particular process steps are comprehensively described elsewhere, Herzog et al., 2016, Grund, 2015, VDI3405, 2013.

Manifold variables affect the LBM process and quality of built parts. As most important actuating variables scan velocity v_s, laser power P_L, hatch distance h_s and layer thickness d_s can be identified, Spierings et al., 2016. These parameters merge to an often used auxiliary value, called volume specific energy density E_v, often shortened as energy density, as given in (1), Kaufmann et al., 2016, VDI3405, 2013.

$$E_v = \frac{P_L}{v_S \cdot h_S \cdot d_S} \qquad (1)$$

All specimens were built on a modified LBM machine of type SLM250HL from SLM Solutions GmbH, equipped with a cw mode 1000 W laser source Rofin FL010S. The melting process was conducted under shielding gas atmosphere with oxygen content below 0.02 %. Argon was used as shielding gas. Base plate heating was set to T_p = 200 °C. For all specimens layer thickness was chosen as constant being d_s = 0.05 mm. All specimens were manufactured using hatch-only scanning strategies without any contour scanning paths. Within the scope of this paper differences in elevations at cube corners or roundings of cube edges are not considered, as the particular focus is set on crack free high density specimens and their hardness as well as the potential of graded mechanical properties. Descriptions of different approaches of various analyses are directly integrated into subsections of the result chapter 3.

2.2. Al-Fe-Ni alloy and its powder raw material

The examined alloy is a high-strength aluminium alloy, provided by the company PLM Powder Light Metals GmbH. Its conventional processing route contains of melt spinning and subsequent hot isostatic

pressing (HIP) followed by extrusion and turning to final shape. Thereby, its distinctive nanostructured microstructure, which develops due to high cooling rates of the melt spinning process, contributes to its high strength mechanical properties, Hummert et al., 2008.

The aluminium alloy contains 5 wt.% Ni, 2.5 wt.% Fe, 2.5 wt.% Cu and in sum 4 wt.% Mn, Mg, Ti, Zr and Mo. For LBM processing the material was gas atomized to nearly spherical powder particles. A particle size distribution from 25 µm to 63 µm was chosen for the process.

2.3. Measurement techniques

Density measurements of LBM samples were conducted by optical measurement with subsequent grey value analysis using a reflected-light microscope Olympus GX51 and Software Olympus Stream. Specimens were hot mounted, grinded and polished parallel to the build direction. In order to avoid falsifications of density values cube border areas did not contribute to porosity counting as the tendency of border related porosity is much higher due to acceleration effects of the scanner system during LBM processing. Hence, appropriate regions of interest (ROI) did not include direct border areas. In case of cracks within a micrograph cracks were also excluded from the ROI.

Hardness measurements were conducted according to DIN EN ISO 6507-1 using Struers DuraScan 70. Mounted and polished density cubes were used for hardness measurements at HV10. At least nine hardness indentations per specimen were executed, arranged in a matrix orientation. Whereas HV10 measurements were applied for non-graded specimens, hardness of graded specimens was analysed using a smaller test force (HV2) due to smaller distances between indentations and resulting higher local resolution.

BSE images for microstructural analysis were received from scanning electron microscopy Zeiss Supra 55 VP at acceleration voltage of 10 kV, aperture of 60 µm and working distance of 8 mm. Same SE microscopy was used for EBSD imaging, applying acceleration voltages of 10 kV at step size of 0.65 µm.

Quasi-static mechanical properties were tested on a servo-hydraulic tensile testing machine Schenck/Instron PC160. Strain gauges were adhered to the specimens for strain to rupture analysis.

2.4. Specimens' geometry

Density cubes with edge length of 10 mm were manufactured on top of an upside down frustum of a pyramid with base area of (1x1) mm as it is schematically illustrated in Fig. 1 (a). This geometry was chosen in order to have a solid connection to the base plate and a simple opportunity to remove parts from the base plate by hand or using pliers. The cube geometry is used for density analysis and hardness tests as well as microstructural analysis.

To analyse process window and resulting microstructures LBM process parameters were set constant for the full building height of a frustum-cube. In order to investigate the potential for manufacturing parts with graded mechanical properties two types of cubes were manufactured, which had distinctive cuboid sections where different LBM parameters with distinctive calculated values of energy densities E_v were applied. Both types are shown schematically in Fig. 1 (b) and (c).

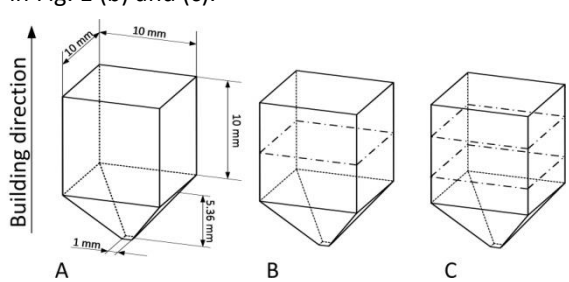

Fig. 1. (a) Non graded cube specimen; (b) two-cuboid specimen; (c) three-cuboid specimen

Tensile test specimens were manufactured according to DIN 50125 A 4 x 20. In contrast to the standard shape a greater shoulder radius of 18 mm was used. Tensile tests were conducted at five specimens in machined condition. Therefore, cylinders with diameter of 10 mm were manufactured by LBM perpendicular to the base plate and machined into final shape.

3. Results

3.1. LBM process window

First cuboids were manufactured using volume specific energy densities between ($25 < E_v < 50$) J/mm³ with varying laser power between ($275 < P_L < 575$) W, scan velocities between ($800 < v_s < 1800$) mm/s and hatch distances between ($0.1 < h_s < 0.19$) mm. Following macroscopic examinations of top surfaces of the cuboids further investigation of part densities were conducted at density cubes between ($30 < E_v < 40$) J/mm³. Due to frequent crack appearance at comparably low E_v values in the former range cubes were also manufactured between ($40 < E_v < 55$) J/mm³.

Microscopic cross section analysis brought up that all specimens within the chosen process window did not show irregular shaped pores, but revealed a microporosity of spherical pores within the part resulting in relative part densities greater than 99 % for crack free cubes. However, the LBM processed material appears to be prone to cracks propagating perpendicular to the building direction. Tendency to crack incidence appears to be higher for low values of E_v. All parts manufactured without base plate heating, which is not included into the calculation of E_v, showed major crack incidence up to bursting of cubes illustrated in Fig. 2. For values of E_v greater than 45 J/mm³ crack incidence disappeared when using platform heating of $T_p = 200$ °C. For further investigations on influence of process parameters on part density and hardness a parameter combination resulting in an energy density E_v of 48.5 J/mm³ was chosen as a reference parameter set.

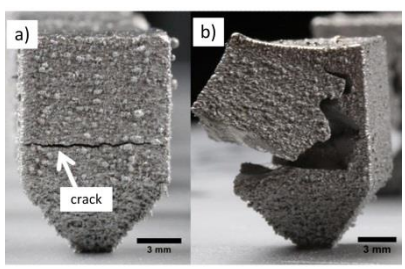

Fig. 2. Examples for crack incidence: a) crack propagating through a part; b) bursting specimen manufactured without base plate heating and low energy density input

3.2. LBM Process parameter dependency on porosity

A variation of process parameters resulting in different energy densities E_v was conducted in order to find an appropriate process window as described in 3.1. Thereafter, the influence of a variation of laser power and scan velocity at nearly constant values of energy density was examined. Therefore, density cubes were manufactured at 13 different parameter combinations. Laser power was varied between ($75 < P_L < 975$) W, scan velocity was varied between ($75 < v_s < 4100$) mm/s. Each combination results in energy density values of E_v around 48.5 J/mm³ as this value turned out to be successfully usable for manufacturing dense and crack

free parts in 3.1. The exact values of E_v resulting from the varied parameter combinations varied between ($47.1 < E_v < 50.0$) J/mm³.

Microscopic cross section analysis revealed that there is a clear dependency between relative part density and chosen process parameters despite same or similar resulting E_v level. The relative part density varies over the chosen parameters as depicted in Fig. 3. Density measurements were examined aiming for relative comparison between densities resulting from different parameter combinations and not for particular determination of absolute values. Therefore, an assumed standard deviation of 0.2 percentage points was used in Fig. 3 following prevenient statistical analysis of uncertainty of density measurements at samples of relative part density greater than 99 %.

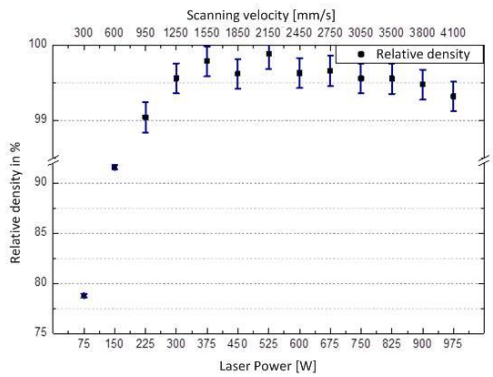

Fig. 3. Relative part density against process parameters laser power and scanning velocity

For low laser powers of 75 W and 150 W not only the porosity values are out of the range of useful part densities but also the shape of the pores is irregular and non-spherical. Additionally, cubes manufactured with these process parameter combinations show cracks propagating through the part. From PL = 225 W upwards the incidence of non-spherical pores is remarkably reduced. Within the range of parameter combinations with laser powers between ($300 < P_L < 750$) W there is a stable process window with low porosity values showing micro-sized pores, predominately of spherical shape. At Laser powers above 800 W the size and number of the spherical pores increase. Fig. 4 illustrates the described trend qualitatively using cross section micrographs.

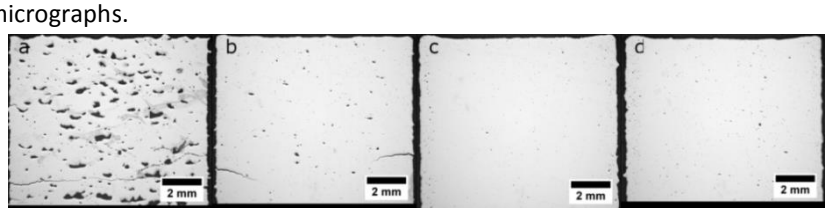

Fig. 4. Cross section micrographs: a) P_L = 150 W; b) P_L = 225 W; c) P_L = 675 W; d) P_L = 900 W

3.3. Microstructure

The characteristic appearance of the microstructure of the LBM processed alloy composition is discussed exemplarily using Fig. 5 which shows BSE-SEM images of a cross section parallel to the building direction at

four different magnifications. The specimen used for microstructural analysis was manufactured using the reference parameter combination from section 3.1.

The microstructure consists of melt lentils connected to each other, which shows distinctive structural constituents. Dendritic structures can be observed in the inner part of a melt lentil, whereas three distinctive regions can be identified at the border areas, which are marked by capitals B, C and D in Fig. 5. Connected to the dendritic region A there is a eutectic region B, which is framed by a layer of globular Aluminium grains with segregations of heavier elements at grain boundaries. This region C is called boundary layer by the authors to be distinguished from the region D which shows additional precipitations (bright flat regions).

EBSD images give an impression of the relevant grain sizes and their distribution and orientation as depicted in Fig. 5. In the inner dendritic region, marked as A, grain sizes from 2.3 µm to 11.3 µm could be observed. Due to the chosen increment of the EBSD measurement of 0.65 µm most parts of the border regions B, C and D could not be indicated within the measurement. However, this stresses the fineness of grains in the border regions of a melt lentil. In consideration of the results of BSE and EBSD analysis it can be summarised that the LBM specimens of the examined Aluminium alloy consists of an inhomogeneous and complex microstructure with alternating regions of very fine and relative coarse grains.

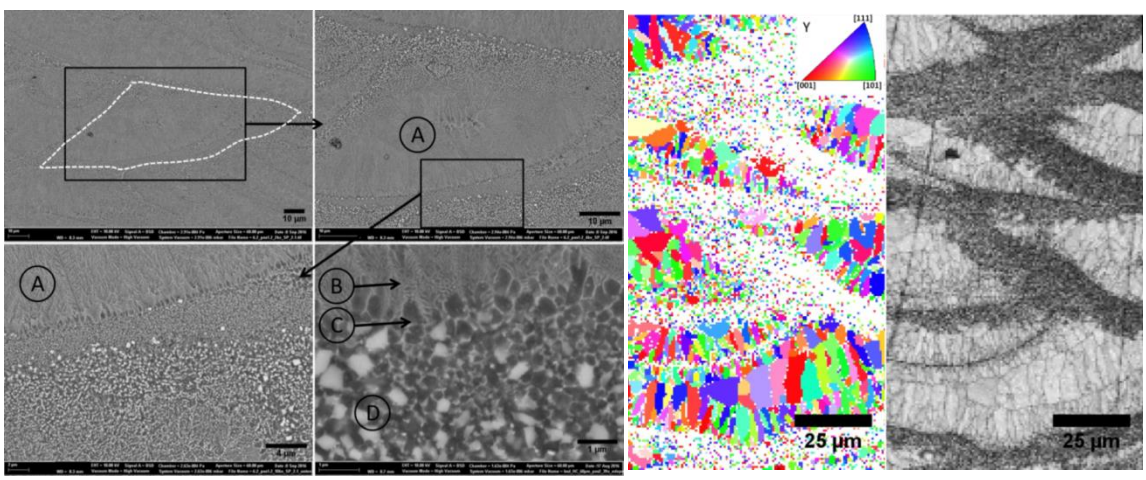

Fig. 5. Left: BSE-images of characteristic microstructure parallel to building direction with distinctive regions: a) dendritic region; b) eutectic region; c) boundary layer; d) fine grained precipitation region; Right: EBSD-images of characteristic microstructure colour-coded and as band contrast

3.4. Hardness

Hardness measurements were conducted at specimens manufactured with parameter combinations of different laser powers and scan velocities but nearly same energy densities E_v, which were analysed for relative part density and described in 3.2 and Fig. 3. The resulting hardness values are shown in Fig. 6. Due to high porosity, parts manufactured with laser power below 200 W were not considered for hardness measurements. With rising laser power or scan velocity, keeping similar values of E_v, a decrease in hardness from around 221 HV10 to around 206 HV10 is noticeable. From parameter combination P_L = 525 W and

v_s = 2150 mm/s on the hardness values stay nearly constant within scattering irrespective of an increase of laser power or scan velocity when resulting in similar E_v values.

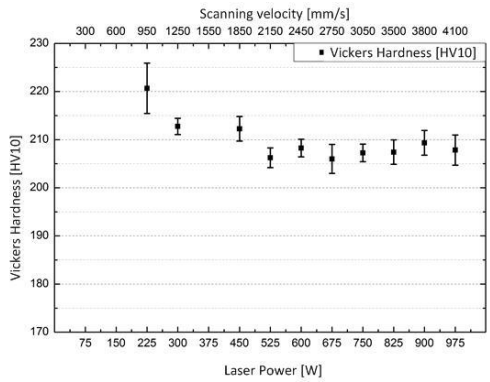

Fig. 6. Vickers hardness HV10 against process parameter combinations resulting in similar values of energy density

Further hardness measurements were conducted at two types of series of process parameter variations as depicted in Table 1 resulting in different energy density values. Cross section analysis revealed that relative part density is greater than 99 % for all parameter combinations resulting from Table 1. The resulting hardness values are shown in Fig. 7. A nearly linear behaviour between hardness and laser power respectively scan velocity can be demonstrated at constant scan velocity respectively constant laser power. The maximum difference of hardness for the investigated parameter combinations is 31 HV10.

Table 1. Field of parameter combinations for hardness variation through variation of energy density input

Process parameter	Series 1 (constant v_s)	Series 2 (constant P_L)
Laser power P_L [W]	varied between	P_{L1} = 375
	375...975	P_{L2} = 675
Scan velocity v_s [mm/s]	v_{s1} = 1550	varied between
	v_{s2} = 2750	750…2750

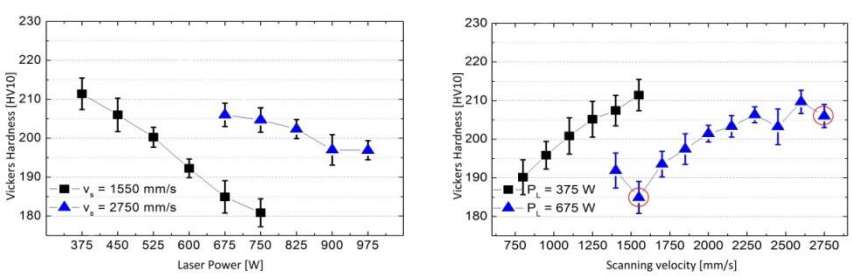

Fig. 7. Hardness against process parameter combinations resulting in various energy densities; values marked in red circles stem not from specimens of the same build job

3.5. Graded hardness

For the investigation of a targeted adjustment of different hardness values within the same specimen, three sets of parameter combinations were chosen from which two are examined here, as they led to the highest or lowest hardness values in hardness investigation in 3.4. The parameter combinations are shown in Table 2.

The two-cuboids specimens were manufactured with combinations of set 1 and set 2 in the way that the upper cuboid was manufactured using set 1, when the lower was manufactured using set 2 and vice versa. The three-cuboid specimens were manufactured with combinations of set 1 and set 2 in the way that the upper and lower cuboid were exposed by the same set, when the cuboid in between was exposed by the other set and vice versa. The height of the middle sections was varied between 300 µm and 3000 µm. Two-cuboid and three-cuboid specimens were built in different build jobs and not on the same base plate. Microscopic cross section analysis revealed similar results in terms of process suitability as for non-graded specimens. However there was a tendency of occurrence of spherical pores alined in a horizontal row at the borderline area between two cuboids of different parameter sets. Additionally, two specimens of the three-cuboid samples showed a crack within the borderline area.

Table 2. Sets of parameter combinations used for graded specimens

	Set 1	Set 2
Laser power P_L [W]	375	750
Scan velocity v_s [mm/s]	1550	1550
Resulting energy density E_v [J/mm³]	48	97

The resulting hardness profile is shown for a two-cuboid specimen and a three-cuboid specimen with a middle section of 1200 µm in Fig. 8. The hardness values of the parameter sets are qualitatively in accordance to the hardness values of cubes analysed in 3.4. Their profile can be described by plateaus of high and low hardness values and transition zones between them, where the hardness drops down to the lower value. The transition zone does not start at the specimen height where the parameter set was changed, which is positioned by the perpendicular lines within the figures. It can be explored that hardness values of the upper cuboid tends to penetrate into the beginning of the subjacent cuboid. This zone is called penetration zone followed by the mentioned transition zone, which is also allocated in the subjacent specimen part. Differences between hardness values of plateaus of same parameter sets for two-cuboid sections and three-cuboid sections can be explored. There was no significant difference between the hardness profiles or the occurrence and width of the transition and penetration zone in dependency of the varied heights of the middle section. Additionally, the section below the middle section of three-cuboid specimens tends to show lower hardness values as the section above.

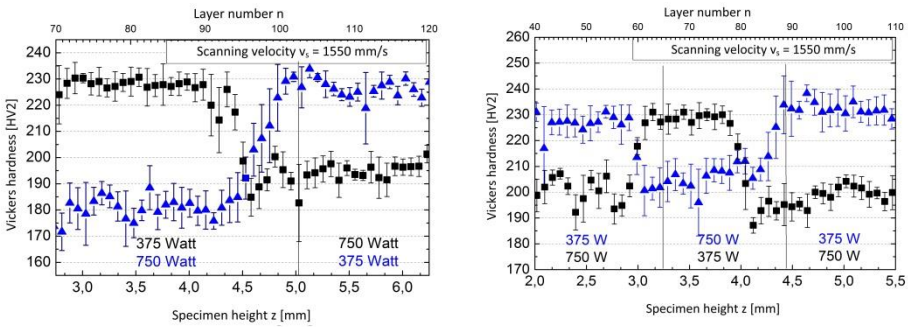

Fig. 8. Hardness profiles for two-cuboid and three-cuboid specimens using two different parameter sets

3.6. Mechanical properties

Specimens for tensile tests were manufactured using a parameter combination resulting in energy density E_v of around 71 J/mm³, as hardness values from measurements in 3.4 were well in between the investigated extrema. Machined specimens showed the following results: Ultimate tensile strength (*UTS*) of 585.58 MPa +/- 8.2 MPa, yield strength of 535.4 MPa +/-25.67 MPa and Young's modulus of 89.97 GPa +/-0.934 GPa. Since strain gauges dropped off from three of five specimens during tensile testing only two values can be shown as strain to rupture results: 1.1 % and 1.3 %.

4. Discussion and outlook

LBM process window examination as well as its extension for further hardness measurements revealed a suitability of the examined Al-Fe-Ni alloy for manufacturing by LBM within a range of energy density values between ($45 < E_v < 97$) J/mm³ when using platform heating of T_p = 200 °C resulting in crack free samples of high relative density greater than 99 %. Mechanical properties show notable high values for *UTS* and yield strength, but only minor strain to rupture. To increase strain to rupture manufacturing of specimens using higher energy density values could be promising as hardness values drops without significant increase of porosity. In addition processing at low values of E_v or without using base plate heating is not recommended within the examined process window, as samples show major crack incidence. These cracks can be attributed to high residual stresses within the specimens due to volume reduction at the phase transition from fluid to solid. Residual stresses are higher at greater thermal gradients according to Kempen et al., 2013, Buchbinder et al., 2014 and Vora et al., 2015. At lower E_v values and at lower preheating temperatures thermal gradients and cooling rates can be assumed to be higher. Hence, residual stresses within the part are more prone to initiate crack propagation at these conditions.

It could be shown that the validity of the auxiliary value E_v as an instrument of comparison is limited to a narrow range of process parameter combinations, as relative density and hardness are not constant over the full range of process parameters, resulting in a constant value of E_v. However, for a range of process parameter combinations resulting in different E_v values this auxiliary value is still a good instrument to show the impact of various thermal gradients resulting from varied energy densities leading to different hardness values. A clear trend for decreasing hardness with increasing energy density E_v can be deduced. Therefore,

the suitability of adjustment of mechanical properties by setting process parameters for the given alloy system can be concluded.

Furthermore, the successful processing of graded specimens with horizontal sections showing distinctive hardness values, dependent on chosen sets of process parameters, depicts the general potential of the Al-Fe-Ni alloy for the production of parts with graded mechanical properties. However, some limits already occurred: There is no sharp transition from one section to the other possible, since a transition zone always develops. Hence, the fineness of a potential horizontal grading is limited by the development of hardness transition zones. Besides, the incidence of pores at the borderline between different sections has to be investigated in further detail as it is a potential weakness and able to act as crack initiation point. Additional examinations have to be done for vertical grading of specimens.

The identification of distinctive microstructural regions within a melt lentil could be explained by the temperature distributions and differences in temperature gradients over the dimension of a meltpool. Simulations of temperature distributions for different materials and different parameters show similar fundamental aspects, Yu and Gu, 2015, Wischeropp et al., 2015, Spierings et al., 2017: Isothermal lines for equidistant temperature ranges, which are drawn around the interaction point of laser exposure, show greater distances from each other with increasing distance from the interaction point. Therefore, the temperature gradient in the inner part of the melt pool is higher than in the outer regions. Spierings et al., 2017 conducted microstructural investigations of an Aluminium-Scandium alloy, where a similar alternating microstructure of fine and coarse regions develops. They explained the development of these regions through the existence of particular intermetallic phases, which are able to act as nucleation sites as long as temperatures are below their dissolution temperatures, which can be the case at the melt pool borders. A similar explanation approach could be applied for the given Al-Fe-Ni alloy where e. g. Al3Ti or Al3Zr phases could act as nucleation sites. This has to be examined in more detail in further work to broaden the understanding for tailored alloy compositions for LBM of high-strength aluminium alloys, aiming for more homogeneous microstructures. Additionally, deeper investigations on the dependency of microstructural sizes and characteristics from LBM process parameters and the energy density will be conducted in further work in order to adjust mechanical properties more precisely by appropriate process parameters.

Acknowledgements

The authors would like to thank ZIM organisation (Central Innovation Program for SMEs) for their financial support through Federal Ministry of Economics and Technology, Germany. They also would like to thank electron microscopy unit (BEEM) of Hamburg University of Technology for its guidance and support at EBSD analysis.

References

Buchbinder, D., Meiners, W., Wissenbach, K., Pirch, N., Schrage, J., 2014. Investigation on reducing distortion by preheating during manufacture of aluminum components using selective laser melting. Journal of Laser Applications 26.

Grund, M. 2015. Implementierung von schichtadditiven Fertigungsverfahren. Mit Fallbeispielen aus der Luftfahrtindustrie und Medizintechnik. Springer Vieweg, Berlin, Germany.

Herzog, D., Seyda, V., Wycisk, E., Emmelmann, C., 2016. Additive manufacturing of metals. Acta Materialia 117, p. 371-392.

Hummert, K., Schattevoy, R., Broda, M., Knappe, M., Müller, R., Beiss, P., Klubberg, F., Schubert, T., Weißgärber, T, 2008. Nanostructured High Strength Aluminium for Automotive Applications. Advances in powder metallurgy & particulate materials 3, 9, p. 161-171.

Karg, M., Ahuja, B., Kuryntsev, S., Gorunov, A., Schmidt, M., 2014. Processability of high strength Aluminium-Copper alloys AW-2022 and 2024 by Laser Beam Melting in Powder Bed, Solid Free Form Fabrication Symposium.

Kaufmann, N., Imran, M., Wischeropp, T., Emmelmann, C., Siddique, S., Walther, F., 2016. Influence of process paramters on the quality of aluminium alloy EN AW 7075 using selctive laser melting (SLM). Physics Procedia 83, p. 918-926.

Kempen, K., Vrancken, B., Thijs, L., Buls, S., Van Humbeeck, J., Kruth, J.-P., 2013. Lowering thermal gradients in Selective Laser melting by pre-heating the baseplate. Solid Freeform Fabrication Symposium.

Kranz J., Herzog, D., Emmelmann C., 2015. Design guidelines for laser additive manufacturing of lightweight structures in TiAl6V4, J. Laser Appl. 27, S14001

Schmidtke, K., Palm, F., Hawkins, A., Emmelmann, C., 2011. Process and mechanical properties: applicability of a scandium modified Al-alloy for laser additive manufacturing, Phys. Procedia 12, p. 369-374.

Spierings, A., Dawson, K., Voegtlin, M., Palm, F., Uggowitzer, P., 2016. Microstructure and mechanical properties of as-processed scandiummodified aluminium using selective laser melting, CIRP Annals, Manufacturing Technology 65., p. 213-126.

Spierings, A., Dawson, K., Heeling, T., Uggowitzer, P., Schäublin R., Palm, F., Wegener, K., 2017. Microstructural features of Sc- and Zr-modified Al-Mg alloys processed by selective laser melting. Materials & Design 115; p. 52‑63.

VDI3405, 2013. Verein Deutscher Ingenieure: Additive Fertigungsverfahren Strahlschmelzen metallischer Bauteile Qualifizierung, Qualitätssicherung und Nachbearbeitung. Beuth Verlag GmbH, Berlin, Germany.

Vora, P., Mumtaz, K., Todd, I., Hopkinson, N, 2015. AlSi12 in-situ alloy formation and residual stress reduction using anchorless selective laser melting. Additive Manufacturing 7, p. 12-19.

Wischeropp, T., Salazar, R., Herzog, D., Emmelmann, C., 2015. Simulation of the effect of different laser beam intensity profiles on heat distribution in selective laser melting. Lasers in Manufacturing Conference 2015.

Yuan, P.; Gu, D., 2015. Molten pool behaviour and its physical mechanism during selective laser melting of TiC/AlSi10Mg nanocomposites: simulation and experiments. Journal of Physics D Applied Physics 48.